MRS Communications

https://doi.org/10.1557/s43579-022-00284-4

MRS Communications

Research Letter

Microstructural evolution at the interface of superconducting thin films and SiC substrate

Michael B. Katz, National Institute of Standards and Technology, Gaithersburg, MD 20899, USA
Chieh-I. Liu, National Institute of Standards and Technology, Gaithersburg, MD 20899, USA; Department of Chemistry and Biochemistry, University of Maryland, College Park, MD 20742, USA
Mattias Kruskopf, National Institute of Standards and Technology, Gaithersburg, MD 20899, USA; Physikalisch-Technische Bundesanstalt, Bundesallee 100, 38116 Brunswick, Germany
Heather M. Hill, Angela Hight Walker, Randolph E. Elmquist, Albert V. Davydov, and Albert F. Rigosi, National Institute of Standards and Technology, Gaithersburg, MD 20899, USA

Address all correspondence to Albert V. Davydov at **albert.davydov@nist.gov**

(Received 29 August 2022; accepted 16 September 2022)

Abstract

Given the importance of fabricating superconducting thin-film device heterostructures, studying material interfaces as a function of processing conditions is warranted. In this work, we assess the interfacial reactions and resulting microstructural evolution at the NbN/SiC interface after thermal annealing. Transmission electron microscopy revealed the diffusion of NbN into the SiC substrate and the formation of NbN nanocrystallites therein induced by the 1400°C treatment. Raman spectroscopy is also employed to gain an understanding of the interface lattices' optical responses.

Introduction

Since its discovery, superconducting NbN has played a key role in several facets of materials science and device fabrication.[1] The modern use of NbN is sustained by the ease with which it can be deposited on a suitable substrate as well as its ability to maintain a superconducting state until above 10 K and for some considerable amount of magnetic flux density (approximately 10 T).[2] Thin films of NbN exhibit some versatility when applying them to quantum computing in the form of single photon detectors, flux quantum circuits, and qubits.[3] Furthermore, these films and their similar counterparts can be deposited onto a variety of substrates including SiC for the purposes of vertical transistors,[4] resistance standards,[5,6] and Josephson junction devices.[7]

Given the extent of functionality for these thin films, knowledge on the interactions between NbN and its corresponding substrate is of vital importance for device engineering. Among available substrates used for material studies, SiC stands out in the following ways: wide bandgaps for semiconductor applications, low loss for THz frequencies, chemical compatibility with other thin films (from insulating to superconducting) fit for quantum communications, and wide commercial availability.[8] For these reasons, interest remains strong in understanding the interfacial interactions between NbN and SiC. Results for NbN/3C-SiC interactions have been recently reported assessing the viability of this heterostructure for hot-electron bolometer mixers and other THz applications.[9] Given this new interest in examining SiC polymorphs and their interactions with thin NbN, it is only fitting that work should be done using 4H-SiC. 4H-SiC is another polymorph known to have superior electronic properties, such as a higher electron and hole mobility as well as a higher Baliga figure of merit,[10] when compared to polymorphs 3C-SiC and 6H-SiC.[11,12]

In this work, NbN films were deposited on 4H-SiC and heat treated at 1400°C. The heat-treated and as-deposited films were examined with transmission electron microscopy (TEM), X-ray diffraction (XRD), scanning electron microscopy (SEM), and Raman spectroscopy to observe the temperature dependence of any interfacial reactions. All depositions were performed via sputtering as with similar processes,[13,14] but it should be noted that there are several varieties of methods for depositing NbN.[2,15,16] The diffusion of Nb and N into the 4H-SiC substrate and subsequent recrystallization therein is reported. We observe the formation of voids, likely resulting from the differences between the coef-ficients of thermal expansion (CTEs) of the interface materials. Data acquired with Raman spectroscopy suggest the forma-tion of carbon-based lattices at the interface for both treatment temperatures.

Results and discussion

Annealing summary and as-deposited samples

Various 4H-SiC substrates were diced from a wafer and subsequently placed in a sputter chamber. After the NbN layer was deposited, specimens were either left as grown, heated to 1400°C. Each of the specimens was then prepared by focused ion beam (FIB) for examination by transmission electron

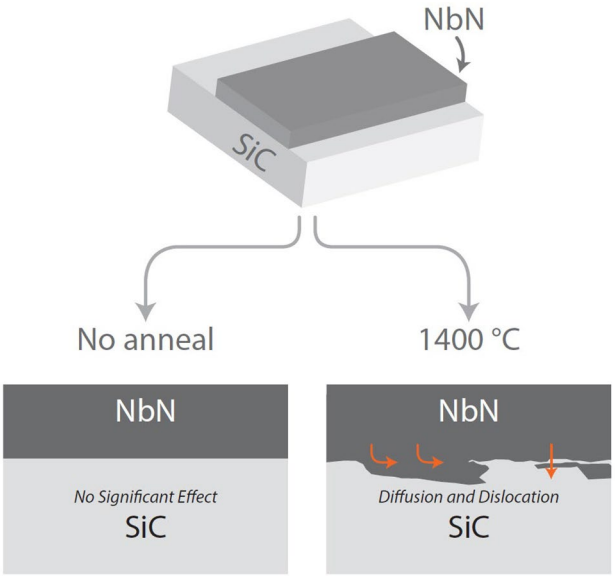

Figure 1. Schematic illustration of the NbN–4H-SiC interface after deposition and the two heat treatments. For the as-deposited interface, no significant reactions were observed. At 1400°C, some of the NbN appears to diffuse into the SiC substrate from the film and forms crystallites.

microscopy (TEM), as described in detail in the "Materials and methods" section. Figure 1 summarizes the results schematically as they will be shown in the following sections. In the case of a lower-temperature 1400°C film, diffusion of NbN and the formation of NbN crystallites and voids within the near-interface region were observed. The NbN generally formed into grains tens of microns in lateral dimension.

In the first case, the as-deposited sample was examined for a baseline comparison to annealed samples. XRD data are acquired and shown in Fig. 2(a), with the data suggesting that the NbN film is amorphous. Figure 2(b) shows a TEM image of the overall polycrystalline NbN film atop the 4H-SiC substrate, with the inset SAED pattern for the NbN film corroborating the polycrystallinity of the NbN.

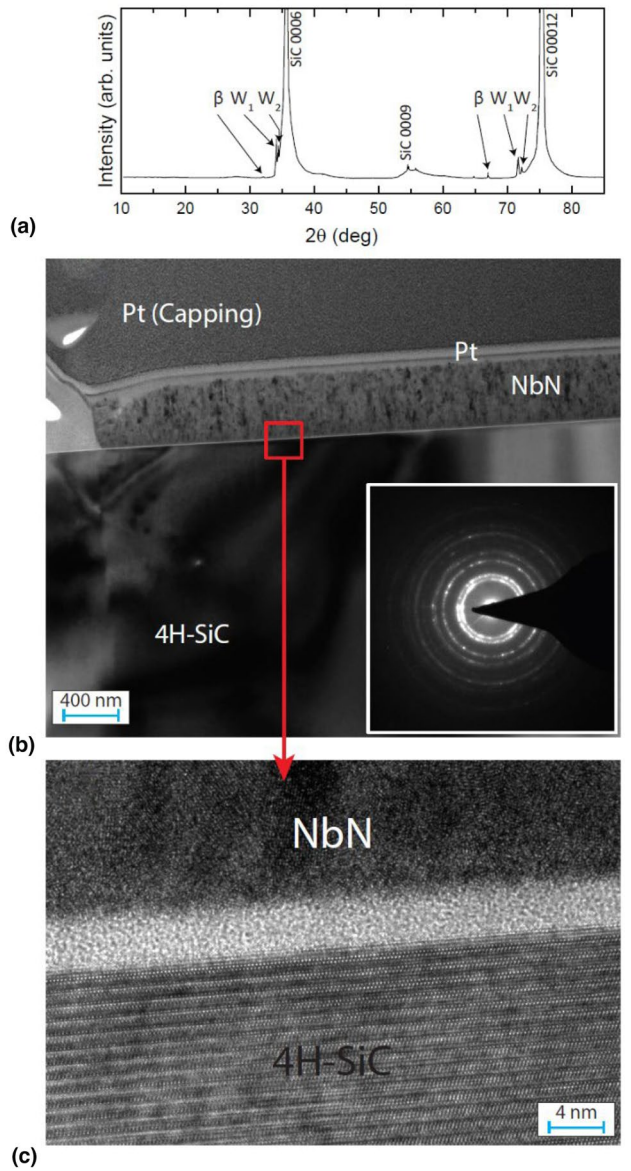

Figure 2. (a) XRD data taken on NbN suggesting an amorphous structure. (b) A TEM image cross-section of the NbN/4H-SiC film stack, with a polycrystalline SAED pattern for the NbN film inset. (c) A higher-magnification TEM image of the indicated region in (b) showing the interface more clearly.

Heat treatment at 1400°C

Heating the film to 1400°C induces a trio of major reactions, both in the NbN film and the 4H-SiC substrate. The extent of the transformations is shown in Fig. 3. The NbN film has completely recrystallized into large grains from its former nanocrystalline state. The grains are approximately 100–300 nm in extent, with single grains spanning the full depth of the film. Also immediately evident, in contrast to the as-grown film, is the separation between the NbN film and the 4H-SiC substrate. It appears not simply delaminated but very rough and uneven at the length scale of the film. This is notable because SiC is generally stable under heat treatments at much higher temperatures. This decomposition of the interfacial region of the 4H-SiC substrate may be partially accounted for by the tendency to relieve increased interfacial energy due to a large mismatch in the CTE during cooling.[17,18]

The third reaction, though, may offer an additional explanation for the extensive degradation of the 4H-SiC at the interface. Examining the near-interfacial region of the 4H-SiC at high magnification reveals a population of faceted nanocrystallites distinct in contrast from the surrounding SiC material. EDS reveals these crystallites to comprise niobium and nitrogen either in part or in full and is likely some phase of Nb_xN_y. The presence of these crystallites and constituent species within the transformed regions of the 4H-SiC suggests the possibility

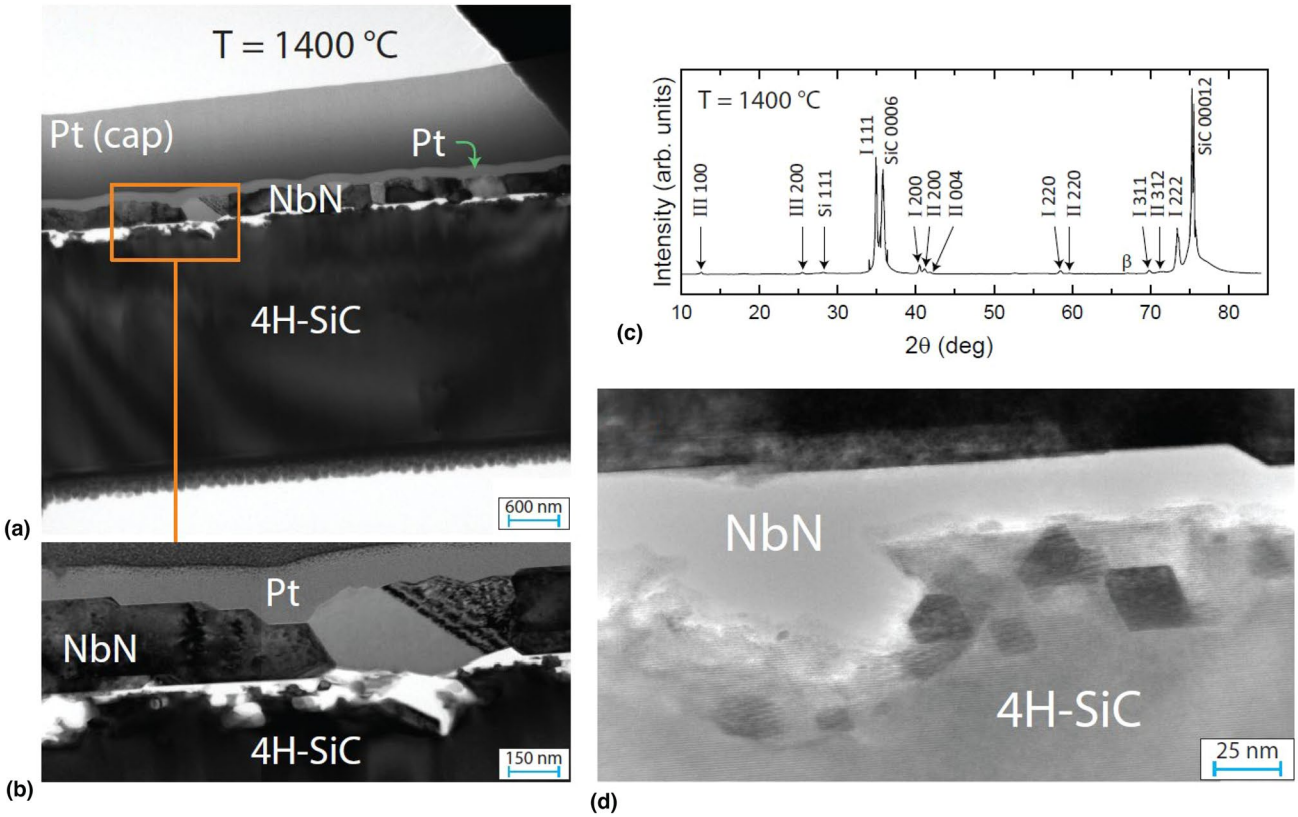

Figure 3. (a) Overview of a cross-section of the film heat treated at 1400°C by TEM and (b) a higher-magnification image of the area called out in (a). The coalescence and subsequent faceting of the NbN film are especially apparent in the grain to the left side of the image. The regions of bright contrast between the NbN film and the 4H-SiC substrate are porosity induced by the heat treatment. (c) XRD data show a mixture of three crystalline NbN phases: (I) δ-NbN (225), (II) tetragonal Nb_4N_3, and (III) cubic primitive NbN_x. The cubic response is very small compared with the other two phases. (d) A high-resolution TEM image of the near-surface region of the 4H-SiC substrate revealing NbN crystallites having formed after migration of Nb and N from the film but before the voids opened up.

that the decomposition of the erstwhile 4H-SiC surface was catalyzed by the presence of and facilitated the migration of these crystallites away from the film and into the substrate.

In the XRD data shown in Fig. 3(c), three distinct crystalline NbN phases are present: (I) δ-NbN (225), which has a characteristic lattice constant $a = 0.446$ nm ,(II) tetragonal Nb_4N_3 (139), with $a = 0.438$ nm and $c = 0.863$ nm, and (III) a primitive cubic NbN_x, with $a = 0.694$ nm, which has scant reports in the literature.[19] Figure 3(d) shows the Nb–N crystallites in detail.

Raman and carbon growth

AQ6 Raman spectroscopy was performed on the samples to get a more comprehensive understanding of the interactions within the interface after the annealing process. Due to the opaque NbN film, the excitation laser was sent through the bottom of the substrate, as has been done in other work to reduce the contribution from the dominant SiC response.[20,21] Rectangular area Raman acquisition maps were also collected across the samples with step sizes of 20 μm in a 5 by 3 raster-style grid, as shown in Fig. 4(a). For each spatial point, a second measurement was taken with a laser focus away from the interface and in the 4H-SiC in order to obtain a pure 4H-SiC signal, as illustrated in Fig. 4(a). The resulting datasets yielded two types of responses, a response from the interface (which includes a response from the 4H-SiC) and one from the 4H-SiC bulk (red and black curves in Fig. 4(b), respectively). A sloped background, resulting from the metallic NbN, was subtracted from all the data. The highest contributing Raman responses for NbN have been measured in other work.[24]

There is a quantifiable difference between the two types of responses, so the differences of the spectra are tabulated and shown in Fig. 4(c) for 1400°C. Within each panel, five example-subtracted spectra are shown along with a solid-averaged curve in light blue. The observed differences in the spectra can be attributed to the vibrational density of states (VDOS) of a proto-graphene layer known as the interfacial buffer layer (IBL), which is still covalently bonded to the 4H-SiC.[22,23] The attribution is more nuanced since there are several crystal formations that can yield similar Raman data. For instance, both NbC and Si_3N_4 have D peaks in similar locations to carbon-based lattices,[24–26] but no other species yield the VDOS behavior seen between 1450 and 1600 cm^{-1}.

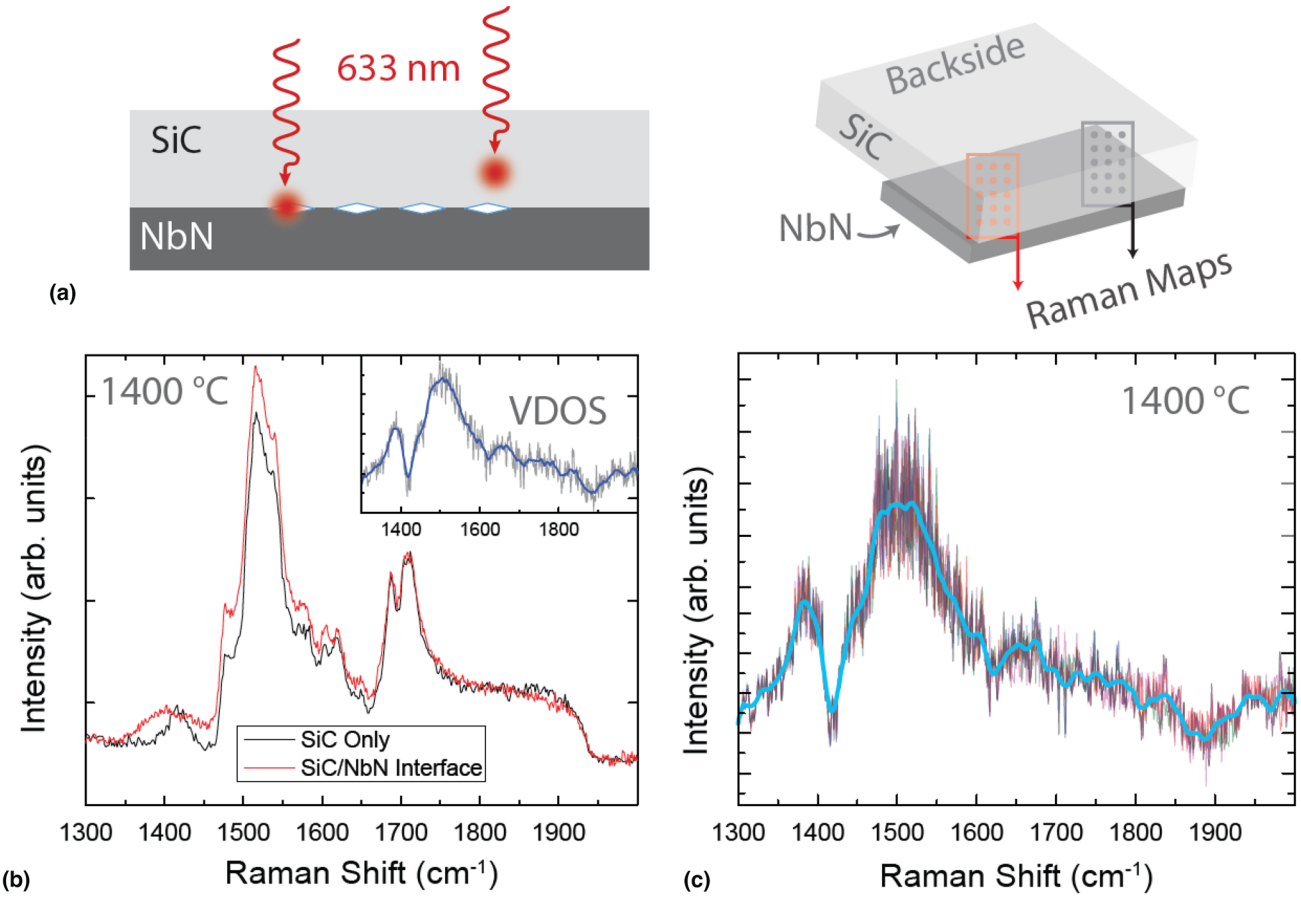

Figure 4. (a) Illustration of the Raman measurement setup, where an incoming laser is focused through the backside of the 4H-SiC substrate on both the interface and the 4H-SiC bulk. (b) An example pair of datasets from the corresponding Raman maps from the 1400°C sample showing a measurable difference between the interface/4H-SiC and pure 4H-SiC (in red and black, respectively). The difference is measurable for all spectra and an example-subtracted spectrum is shown in the inset. (c) Several examples of differences in the Raman spectra are attributable to the VDOS of the buffer layer seen when carbon-based lattices form on the surface of 4H-SiC.

These analyses provide additional insights into the interactions and changes that have occurred at the NbN/4H-SiC interface.

All 1400°C data in the spectral neighborhood of the 2D peak showed no measurable responses. First, since the 2D peak was not vis-ible for all spectra, a very high level of disorder of the new lattice should be expected. Second, this disorder was further validated by the relatively strong D peak (that is, the ratio of I_D/I_{2D} is much greater than 1). Third, there were a complete lack of additional peaks typically seen in niobium-based or silicon-based lattices in the same neighborhood with similar intensities as the 2D peak. These observations, plus the agree-ing data from the VDOS, indicate that a carbon-based lat-tice was the dominant new formation at the interface. These analyses provide additional insights into the interactions and changes that have occurred at the NbN/4H-SiC interface.

Conclusion

In this work, depositions of NbN films on 4H-SiC were examined with transmission electron microscopy (TEM) and other related techniques after heat treatments at 1400°C as well as as-grown to assess the extent of interfacial interactions and any possible temperature-dependent behavior. Overall, diffusion of NbN into and the nucleation of crystallites of NbN within the near-surface regions of the 4H-SiC substrate were observed at 1400°C. Additionally, Raman measurements showed the effects on the 4H-SiC by revealing a carbon-based lattice formation at the interface. These observations have clarified the extent to which interfacial interactions are temperature dependent.

Materials and methods

SiC substrates were prepared and diced from on-axis 4H-SiC (0001) semi-insulating wafers as in other similar work.[27]

A Denton Vacuum Discovery 550 (see Acknowledgments) was used to deposit NbN on 4H-SiC substrates. The process

began when the minimum vacuum of 1.33×10^{-3} Pa was met. Flow rates correspond to gases at standard temperature and pressure. The deposition process for superconducting NbN contains seven steps. (1) Nitrogen and argon gas flow at 120 cm^{-3}/min and 20 cm^{-3}/min, respectively, for 20 min (to clean the chamber). (2) Pre-sputtering ensures removal of possible gaseous contaminants on the sputter targets. For 10 min, argon gas flows at 50 cm^{-3}/min, while the Nb sputter target is being cleaned (DC ion source, 2 W). (3) A second pre-sputtering step with nitrogen and argon gas flow at 3 cm^{-3}/min and 50 cm^{-3}/min, respectively, for 5 min (Nb DC ion source, 1.5 W). (4) Nb sputtered in the same conditions as step 3 to promote growth of superconducting NbN (10 min). (5) Chamber flush for 1 min using argon gas flow at 50 cm^{-3}/min. (6) Pre-sputter for 5 min using argon gas flow at 50 cm^{-3}/min (Pt DC ion source, 0.2 W). (7) Pt is deposited as a protective capping layer to protect it from oxidation (same conditions as step 6). This deposition yields 330 nm NbN and 50 nm Pt. In corresponding TEM images, a significantly thicker, second Pt layer is deposited as part of the TEM sample preparation method.

The annealing step at 1400°C was performed with a background argon gas environment (originating from a 99.999% liquid argon source) at 104 kPa (slightly above atmospheric pressure). The ramping rate was approximately 90°C/min, and the annealing began with a gradual heating to 1050°C followed by the second segment of heating to 1400°C. This process occurs over about 10 min. The cooling process occurs after annealing at the maximum temperature for 30 min, with a cooling rate of 90°C/min. The annealing is performed with a graphite-lined resistive element furnace [Materials Research Furnaces LLC (see Acknowledgments)] that is cooled by chilled water. Pumping and backfilling are done with a mass flow valve and a multistage roots dry pump. Some samples were not annealed at all.

Raman measurements were performed with a Renishaw InVia micro-Raman spectrometer (see Acknowledgments) using a 633-nm wavelength excitation laser source. The spectra were collected using a backscattering configuration, 300-s acquisition time, 1-μm spot size, 50× objective, 1.7-mW power, and 1800-mm^{-1} grating. Rectangular acquisition maps were also collected with step sizes of 20 μm in a 5 by 3 raster-style grid.

AQ7 Cross-sectional TEM specimens were prepared by focused ion beam milling in a FEI Nova NanoLab Dual-Beam FIB using a gallium ion beam. Pt capping layers were used to protect the film from the ion beam during processing. TEM observation was performed in a FEI Titan TEM under a 300-kV accelerating voltage.

Acknowledgments

The authors thank D. B. Newell, S. Payagala, G. Fitzpatrick, A. L. Levy, and E. C. Benck for assistance with the internal NIST review process. Commercial equipment, instruments, and materials are identified in this paper in order to specify the experimental procedure adequately. Such identification is not intended to imply recommendation or endorsement by the National Institute of Standards and Technology or the United States government nor is it intended to imply that the materials or equipment identified are necessarily the best available for the purpose.

Author contributions

C-IL, REE, and MK prepared samples. MBK performed electron microscopy measurements and analysis. AVD performed x-ray diffraction and analysis. AFR, AHW, REE, and AVD assisted with the analyses, support, and general project oversight. The manuscript was written through contributions of all authors. All authors have given approval to the final version of the manuscript.

Funding

Work presented herein was performed, for a subset of the authors, as part of their official duties for the United States Government. Funding is hence appropriated by the United States Congress directly.

Data availability

Data presented herein are available from the corresponding author upon reasonable request.

Declarations

Conflict of interest

The authors declare no conflict of interest.

References

1. G. Aschermann, E. Friederich, E. Justi, J. Kramer, Supraleitfahige Verbindungen mit extrem hohen Springtemperaturen. Physik Z. **42**, 349 (1941)
2. G.Y. Wang, Z. Zhu, X.Y. Yang, L. Dong, H.Y. Ma, H.H. Sun, A.M. Li, D.D. Guan, D. Qian, C. Liu, Y.Y. Li, J.F. Jia, Atomically flat superconducting NbN thin films grown on $SrTiO_3$ (111) by plasma-assisted MBE. APL Mater. **5**, 126107 (2017)
3. Y. Nakamura, H. Terai, K. Inomata, T. Yamamoto, W. Qiu, Z. Wang, Superconducting qubits consisting of epitaxially grown NbN/AlN/NbN Josephson junctions. Appl. Phys. Lett. **99**, 212502 (2011)
4. C.O. Bozler, Current prospects for the permeable base transistor. Surf. Sci. **174**, 487 (1986)
5. A.F. Rigosi, R.E. Elmquist, The quantum Hall effect in the era of the new SI. Semicond. Sci. Technol. **34**, 093004 (2019)
6. T. Oe, A.F. Rigosi, M. Kruskopf, B.Y. Wu, H.Y. Lee, Y. Yang, R.E. Elmquist, N.H. Kaneko, D.G. Jarrett, Comparison between NIST graphene and AIST GaAs quantized Hall devices. IEEE Trans. Instrum. Meas. **69**, 3103–3108 (2019)
7. R. Simmonds, K. Lang, D. Hite, S. Nam, D. Pappas, J. Martinis, Decoherence in Josephson phase qubits from junction resonators. Phys. Rev. Lett. **93**, 077003 (2004)
8. R. Yakimova, E. Janzén, Current status and advances in the growth of SiC. Diam. Relat. Mater. **9**, 432–438 (2000)
9. D. Dochev, V. Desmaris, A. Pavolotsky, D. Meledin, Z. Lai, A. Henry, E. Janzén, E. Pippel, J. Woltersdorf, V. Belitsky, Growth and characterization of

epitaxial ultra-thin NbN films on 3C-SiC/Si substrate for terahertz applications. Supercond. Sci. Technol. **24**, 035016 (2011)
10. B.J. Baliga, Power semiconductor device figure of merit for high-frequency applications. IEEE Electron Dev. Lett. **10**, 455–457 (1989)
11. T. Kimoto, J. Cooper, *Fundamentals of Silicon Carbide Technology: Growth, Characterization, Devices and Applications* (Wiley, Singapore, 2014). https://doi.org/10.1002/9781118313534
12. W. Ching, Y.-N. Xu, P. Rulis, L. Ouyang, The electronic structure and spectroscopic properties of 3C, 2H, 4H, 6H, 15R and 21R polymorphs of SiC. Mater. Sci. Eng. A **422**, 147–156 (2006)
13. M. Kruskopf, A.F. Rigosi, A.R. Panna, D.K. Patel, H. Jin, M. Marzano, M. Berilla, D.B. Newell, R.E. Elmquist, Two-terminal and multi-terminal designs for next-generation quantized Hall resistance standards: contact material and geometry. IEEE Trans. Electron Dev. **66**, 3973–3977 (2019)
14. M. Kruskopf, A.F. Rigosi, A.R. Panna, M. Marzano, D.K. Patel, H. Jin, D.B. Newell, R.E. Elmquist, Next-generation crossover-free quantum Hall arrays with superconducting interconnections. Metrologia **56**, 065002 (2019)
15. K. Senapati, N.K. Pandey, R. Nagar, R.C. Budhani, Normal-state transport and vortex dynamics in thin films of two structural polymorphs of superconducting NbN. Phys. Rev. B **74**, 104514 (2006)
16. D.S. Katzer, N. Nepal, M.T. Hardy, B.P. Downey, D.F. Storm, E.N. Jin, R. Yan, G. Khalsa, J. Wright, A.C. Lang, T.A. Growden, V. Gokhale, V.D. Wheeler, A.R. Kramer, J.E. Yater, H.G. Xing, D. Jena, D.J. Meyer, Molecular beam epitaxy of transition metal nitrides for superconducting device applica-tions. Phys. Status Solidi A **217**, 1900675 (2020)
17. X.-G. Lu, M. Selleby, B. Sundman, Calculations of thermophysical properties of cubic carbides and nitrides using the Debye–Gruneisen model. Acta Mater. **55**, 1215–1226 (2007)
18. F. Mercier, S. Coindeau, S. Lay, A. Crisci, M. Benz, T. Encinas, R. Boichot, A. Mantoux, C. Jimenez, F. Weiss, E. Blanquet, Niobium nitride thin films deposited by high temperature chemical vapor deposition. Surf. Coat. Technol. **260**, 126–132 (2014)
19. M. Benkahoul, E. Martinez, A. Karimi, R. Sanjinés, F. Lévy, Structural and mechanical properties of sputtered cubic and hexagonal NbN_x thin films. Surf. Coat. Technol. **180**, 178–183 (2004)
20. F. Fromm, P. Wehrfritz, M. Hundhausen, T. Seyller, Looking behind the scenes: Raman spectroscopy of top-gated epitaxial graphene through the substrate. New J. Phys. **15**, 113006 (2013)
21. A.F. Rigosi, D. Patel, M. Marzano, M. Kruskopf, H.M. Hill, H. Jin, J. Hu, A.R.H. Walker, M. Ortolano, L. Callegaro, C.T. Liang, Atypical quantized resistances in millimeter-scale epitaxial graphene pn junctions. Carbon **154**, 230–237 (2019)
22. H.M. Hill, A.F. Rigosi, S. Chowdhury, Y. Yang, N.V. Nguyen, F. Tavazza, R.E. Elmquist, D.B. Newell, A.R.H. Walker, Probing the dielectric response of the interfacial buffer layer in epitaxial graphene via optical spectroscopy. Phys. Rev. B **96**, 195437 (2017)
23. F. Fromm, M.H. Oliveira, A. Molina-Sánchez, M. Hundhausen, J.M.J. Lopes, H. Riechert, L. Wirtz, T. Seyller, Contribution of the buffer layer to the Raman spectrum of epitaxial graphene on SiC(0001). New J. Phys. **15**, 043031 (2013)
24. A. Tolosa, B. Krüner, S. Fleischmann, N. Jäckel, M. Zeiger, M. Aslan, I. Grobelsek, V. Presser, Niobium carbide nanofibers as a versatile precursor for high power supercapacitor and high energy battery electrodes. J. Mater. Chem. A **4**, 16003–16016 (2016)
25. I. AlShibane, J.S. Hargreaves, A.L. Hector, W. Levason, A. McFarlane, Synthesis and methane cracking activity of a silicon nitride supported vanadium nitride nanoparticle composite. Dalton Trans. **46**, 8782 (2017)
26. J.Z. Jiang, K. Ståhl, R.W. Berg, D.J. Frost, T.J. Zhou, P.X. Shi, Structural characterization of cubic silicon nitride. EPL **51**, 62 (2000)
27. A.R. Panna, I. Hu, M. Kruskopf, D.K. Patel, D.G. Jarrett, C. Liu, S.U. Payagala, D. Saha, A.F. Rigosi, D.B. Newell, C.-T. Liang, R.E. Elmquist, Graphene quantum Hall effect parallel resistance arrays. Phys. Rev. B 103, 075408 (2021)